AIP | Journal of Applied Physics

Morphology and Curie temperature engineering in crystalline La0.7Sr0.3MnO3 films on Si by pulsed laser deposition

Rajashree Nori, S. N. Kale, U. Ganguly, N. Ravi Chandra Raju, D. S. Sutar, R. Pinto, and V. Ramgopal Rao

Citation: Journal of Applied Physics **115**, 033518 (2014); doi: 10.1063/1.4862909
View online: http://dx.doi.org/10.1063/1.4862909
View Table of Contents: http://scitation.aip.org/content/aip/journal/jap/115/3?ver=pdfcov
Published by the AIP Publishing

Articles you may be interested in

Anisotropic low field magnetoimpedance in (001) oriented La0.7Sr0.3MnO3 thin films
J. Appl. Phys. **113**, 17C730 (2013); 10.1063/1.4795714

Enhanced low field magnetoresistance of Al 2 O 3 - La 0.7 Sr 0.3 MnO 3 composite thin films via a pulsed laser deposition
J. Appl. Phys. **96**, 1568 (2004); 10.1063/1.1763237

Influence of the morphology on the magneto-transport properties of laser-ablated ultrathin La 0.7 Ba 0.3 MnO 3 films
J. Appl. Phys. **90**, 1429 (2001); 10.1063/1.1380217

Magnetotransport of La 0.7 Sr 0.3 MnO 3 /SrTiO 3 multilayers with ultrathin manganite layers
J. Appl. Phys. **89**, 6973 (2001); 10.1063/1.1362649

Microstructure and magnetic properties of strained La 0.7 Sr 0.3 MnO 3 thin films
J. Appl. Phys. **88**, 4257 (2000); 10.1063/1.1309040

Reuse of AIP Publishing content is subject to the terms at: https://publishing.aip.org/authors/rights-and-permissions. Download to IP: 130.102.82.169 On: Tue, 04 Oct 2016 05:47:48

Morphology and Curie temperature engineering in crystalline $La_{0.7}Sr_{0.3}MnO_3$ films on Si by pulsed laser deposition

Rajashree Nori,[1,a)] S. N. Kale,[2] U. Ganguly,[1] N. Ravi Chandra Raju,[1] D. S. Sutar,[3] R. Pinto,[1] and V. Ramgopal Rao[1]
[1]*Centre of Excellence in Nanoelectronics, Department of Electrical Engineering, Indian Institute of Technology-Bombay (IIT-B), Mumbai 400076, India*
[2]*Department of Applied Physics, Defence Institute of Advanced Technology (DIAT), Pune 411025, India*
[3]*Central Surface Analytical Facility, Indian Institute of Technology-Bombay (IIT-B), Mumbai 400076, India*

(Received 24 November 2013; accepted 8 January 2014; published online 21 January 2014)

Of all the colossal magnetoresistant manganites, $La_{0.7}Sr_{0.3}MnO_3$ (LSMO) exhibits magnetic and electronic state transitions above room temperature, and therefore holds immense technological potential in spintronic devices and hybrid heterojunctions. As the first step towards this goal, it needs to be integrated with silicon via a well-defined process that provides morphology and phase control, along with reproducibility. This work demonstrates the development of pulsed laser deposition (PLD) process parameter regimes for dense and columnar morphology LSMO films directly on Si. These regimes are postulated on the foundations of a pressure-distance scaling law and their limits are defined post experimental validation. The laser spot size is seen to play an important role in tandem with the pressure-distance scaling law to provide morphology control during LSMO deposition on lattice-mismatched Si substrate. Additionally, phase stability of the deposited films in these regimes is evaluated through magnetometry measurements and the Curie temperatures obtained are 349 K (for dense morphology) and 355 K (for columnar morphology)—the highest reported for LSMO films on Si so far. X-ray diffraction studies on phase evolution with variation in laser energy density and substrate temperature reveals the emergence of texture. Quantitative limits for all the key PLD process parameters are demonstrated in order enable morphological and structural engineering of LSMO films deposited directly on Si. These results are expected to boost the realization of top-down and bottom-up LSMO device architectures on the Si platform for a variety of applications.
© *2014 AIP Publishing LLC*. [http://dx.doi.org/10.1063/1.4862909]

I. INTRODUCTION

Over last few decades, the silicon industry has overcome many technological hurdles through innovations in process engineering and successful introduction of new materials into conventional device fabrication flow.[1,2] Exploring new materials that overcome limitations of all-silicon devices and which enhance device functionality have been actively pursued.[3–6] In this context, much work is yet to be done to integrate the versatile colossal magnetoresistant (CMR) manganites on silicon. These materials are manganese oxides of the formula: $R_{1-x}A_xMnO_3$, where R = a rare-earth element, A = a divalent ion; and typically exhibit a large change in their resistance on the application of a magnetic field, also known as magnetoresistance (*MR*).[7,8] Some of them are known to become ferromagnetic at or above a certain value of "x" (i.e., A-doping percentage) and undergo a transition from ferromagnetic to paramagnetic state at their Curie temperature (T_c), which is closely linked to their metal to insulator transition temperature (T_p). Of the all the CMR manganites, $La_{0.7}Sr_{0.3}MnO_3$ (LSMO) is of particular interest since it exhibits high *MR* with bulk T_c above room temperature (360 K) and demonstrates lowest resistivity with $\rho_{4.2K} \approx 8\,m\Omega$ cm.[8,9] For its room-temperature CMR properties, LSMO has been investigated for spintronic applications to serve as an active layer in *MR* sensors and spin valves.[10,11] Additionally, LSMO thin films are being considered for fabrication of hybrid transistors and p-n junctions.[12–14] Known to have 100% spin polarized carriers, it has been successfully used in conjunction with III-V semiconductors as well as organic semiconductors for spin injection and transport.[15,16] With a unique combination of room temperature properties, such as high intrinsic hole concentration, low bandgap, high *MR*, and 100% spin polarization, integration of LSMO on Si platform is envisioned to open up multiple device opportunities.

The primary challenge in depositing LSMO on Si lies in the high degree of structural mismatch between the two systems. They differ in their thermal conductivity,[17,18] thermal coefficient of expansion,[19,20] crystal structure, and lattice constant values—all parameters which can have a significant impact on the growth mode of a film, especially at elevated temperatures. The reported lattice constant for LSMO (perovskite structure) films is ~3.876 Å, which effectively corresponds to the Mn-O-Mn bond length.[9,21] With the Si (diamond cubic structure) lattice constant value to be 5.431 Å,[22] lattice mismatch between the two systems can be deduced to be 28.63%. This suggests the outcome of LSMO deposition on Si to be a polycrystalline film with distinct island morphology obtained via Volmer-Weber growth mode.[23] However, one may note that LSMO (with x = 0.3) is known to have a

a)Author to whom correspondence should be addressed. Electronic mail: rajsre@ee.iitb.ac.in

 © 2014 AIP Publishing LLC

Reuse of AIP Publishing content is subject to the terms at: https://publishing.aip.org/authors/rights-and-permissions. Download to IP: 130.102.82.169 On: Tue, 04 Oct 2016 05:47:48

rhombohedral perovskite structure belonging to R-3 c space group. In this description of the unit cell, wherein the lattice 3-fold symmetry lies along the body diagonal, its lattice constant is reported to be 5.506 Å.[24] Considering this value, lattice mismatch with Si reduces to 1.4%, thereby suggesting the possibility of obtaining strained, textured films of LSMO on Si with careful process engineering.

Few studies report initial efforts in deposition of LSMO on a Si-based platform via sputtering and pulsed laser deposition (PLD) techniques. Some employ thick buffer layers to overcome lattice mismatch, while others have attempted direct deposition.[19,20,25,26] However, process tuning in these techniques remains empirical and requires optimization for achieving stoichiometric LSMO films. One study reports success in obtaining epitaxial LSMO films on Si(100) substrate using PLD, although no physical properties of the deposited film other than x-ray diffraction results are provided.[27] Most significantly, all reports so far point to growth of polycrystalline films on Si, having T_c values to be much lower than that of bulk LSMO, with highest value reported to be only 325 K.[28,29] T_c is indicative of the morphological, structural, and compositional quality of deposited manganite films, since it is highly sensitive to residual strain and non-uniformities.[20,30] Hence, obtaining a film T_c value close to the bulk value of 360 K is imperative towards ensuring LSMO phase purity and compositional uniformity on Si for device applications. Another vital requirement for device applications is control over film morphology. Conventional top-down device fabrication approach demands film morphology to be free of pin-holes and inter-granular separation, while the new emerging bottom-up device fabrication approach requires the film to consist of an array of separated islands. Very few studies discuss morphology control of multi-cationic films,[31–33] and fewer still focus on LSMO film morphology control.[34,35] Through our work here, we demonstrate success in achieving high T_c films of LSMO with complete morphology control and process reproducibility directly on Si. We quantitatively define separate PLD process parameters regimes to obtain dense and columnar LSMO films on Si, suited for top-down and bottom-up device architectures, respectively.

We chose to deposit LSMO on Si using PLD—a commonly used technique for deposition of multi-cationic oxides, reported to be effective in producing smooth and stoichiometric films.[36] This technique has a large number of process variables (described in experimental section), which often need to be optimized for a given film-substrate system through empirical methods. While this increases process complexity, it also provides multiple handles for process control. The objectives of this work are (i) to establish a theoretical framework for morphology development during PLD of LSMO on Si (ii) to define PLD process windows for LSMO films on Si with complete morphology and phase control. Building on previously reported models on film growth using PLD, we first establish primary process conditions for morphology development on Si. These conditions are experimentally validated and also simultaneously investigated for phase development. Based on obtained results, PLD process parameter zones for high-T_c, dense and columnar LSMO films on Si are thereafter identified.

II. EXPERIMENTAL DETAILS

All films were deposited on ~1 cm × 2 cm, RCA-cleaned, n-type Si(100) wafer pieces; with a 10:1 HF dip just prior to substrate loading. A KrF excimer laser operating at $\lambda = 248$ nm with 30 ns pulse width was used for all the depositions. Key PLD process parameters were identified to be as follows: laser energy density (*ED*), laser pulse repetition rate (*RR*), laser spot size (*SS*), oxygen ambient pressure (*P*), substrate-target distance (*D*), and deposition temperature (*T*). These parameters were systematically varied over different process sets, with multiple deposition runs done in each set to ensure repeatability. Constant time depositions were done in each set with substrate centered normal to the plume axis. Cross section scanning electron microscopy along the vertical and horizontal axes of the substrate was performed to ascertain average thickness of deposited films—found to range from 200 nm to 700 nm across process sets. Constant thickness (~50 nm) films of selected process sets were also deposited for comparison of their physical and chemical properties. Inspection of film surface morphology and film cross-section was done using the Raith 150 Two Scanning Electron Microscope. This tool consists of a Zr field emission gun with a resolution of 5 nm at 10 kV operating voltage. Each sample was imaged at 10 kV, without any metal/conducting layer coat. Structural characterization of deposited films was done using the Panalytical X'Pert PRO X-ray diffractometer with Cu $K\alpha_1$ radiation (1.5406 Å), operating at 40 kV and 30 mA. θ–2θ scans in the 20°–60° range were collected in continuous mode with a step size of 0.017° and step time of 5.16 s. Obtained patterns were corrected for Cu $K\alpha_2$ noise and further analyzed using X'Pert High Score Plus software. Analysis of the target XRD pattern (obtained prior to deposition experiments) confirmed the target structure to match with rhombohedral $La_{0.7}Sr_{0.3}MnO_3$ crystal system with lattice parameters as given in the ICDD database.[24] Similar procedure was followed to obtain ICDD database match for XRD data of deposited films.

Quantum Design's Magnetic Property Measurement System (MPMS) − 010 was used to measure the Curie temperature of all LSMO films. The system consists of an RF superconducting quantum interference device (SQUID) amplifier system for magnetic moment detection, enabling it to measure magnetic moments as low as 10^{-8} emu from a thin film sample when vibrated in an applied magnetic field. For every measurement, a 5 mm × 5 mm sample piece was mounted on a quartz holder and thereafter inserted into the measurement chamber. Sample moment was measured in the temperature range of 390 K to 5 K, as the sample cooled in an applied field of 50 Oe. Temperature ramp down rate was set at 5 K/min, with peak vibration amplitude of 5 mm and averaging time of 5 s, under continuous data acquisition mode. From the obtained magnetization *M* vs. temperature *T* curve, Curie temperature T_c was extracted by extrapolation upto $\chi^{-1} = 0$, as per the Curie-Weiss law.[34] Photoelectron spectroscopy measurements were also performed on selected

Reuse of AIP Publishing content is subject to the terms at: https://publishing.aip.org/authors/rights-and-permissions. Download to IP: 130.102.82.169 On: Tue, 04 Oct 2016 05:47:48

LSMO film samples in a Thermo VG Scientific Multilab system. The system is equipped with a monochromatic Al (Kα) X-rays source at 1486.6 eV and concentric hemispherical electron energy analyzer. The measurements were done at a base pressure of $<1.0 \times 10^{-7}$ Pa with constant analyzer pass energy of 25 eV giving overall energy resolution of 0.5 eV. In order to probe the as-deposited surface stoichiometry of the films, XPS spectra were recorded without Ar^+ ion etch and thereafter analysed using the peak fitting software XPSpeak 4.1. Each core level spectrum was decomposed into individual Gaussian-Lorentzian peaks after a Shirley background subtraction. The internal calibration of BE scale was done by referring to the adventitious carbon peak (C1s) at 284.6 eV.

III. THEORETICAL FRAMEWORK

There are numerous reports in literature on PLD of LSMO and $YBa_2Cu_3O_{7-x}$ (YBCO) films on their lattice matched substrates such $SrTiO_3$ (STO), $LaAlO_3$ (LAO), and MgO. Studies range from empirical methods to development of models such as *P-T* diagram[37] and *P-D* scaling laws[33] (*P, D, T*, and other PLD process parameters are defined in the experimental section). Qualitative understanding of *P-T* and *P-D* laws can be achieved by considering the fact that oxygen pressure during deposition can affect the spatial and velocity distribution of the travelling plume species. For a given film-substrate system, an optimal velocity of the arrival species is desired such that it satisfies the conditions for surface activation of ad-atoms for film nucleation. Substrate temperature (*T*) can provide additional energy to overcome the barrier for nucleation for a given system and hence, can be tuned along with pressure *P* to achieve high quality films.[36] Similarly, the *P-D* model was first developed in 1992 by Kim *et al.* for PLD of superconducting material YBCO on MgO (100) substrates.[33] Koubaa *et al.* showed that LSMO films deposited on lattice matched substrates such as STO and LAO using PLD followed the *P-D* scaling law, with the smoothest films obtained at low *P* and *D*.[34,38] In their reports on morphology control of LSMO films on STO substrates, they empirically derived the law constants for LSMO deposition on STO as follows:[34]

$$PD^3 = 31894\ldots \text{m Torr cm}^3 @ T = 570\,^{\circ}\text{C}, \quad (1)$$

$$PD^3 = 18225\ldots \text{m Torr.cm}^3 @ T = 670\,^{\circ}\text{C}. \quad (2)$$

Film morphologies obtained in their experiments were correlated with the "microstructure zones model" for sputtered film morphology. *P-D* zones for columnar and dense morphology were qualitatively defined, where columnar morphology is obtained for PD^3 product much greater than the PD^3 constant and dense morphology is obtained at PD^3 conditions close to or lower than the constant value. In all these studies, *P-D* relationship was derived for epitaxial film growth between lattice matched systems. For device applications, it is of interest to investigate the relevance of this law to lattice mismatched systems of LSMO and Si as well. To begin with, PD^3 law constants for LSMO on Si need to be calculated for our experimental validation. We do so using Eqs. (1) and (2), wherein the ratio of law constants for a 100 °C rise in temperature was found to be equal to 0.5714. Constants for other deposition temperatures used in this work are thereby calculated to be

$$PD^3 = 15597\ldots \text{m Torr.cm}^3 @ T = 700^{\circ}\text{C}, \quad (3)$$

$$PD^3 = 11601\ldots \text{m Torr.cm}^3 @ T = 750^{\circ}\text{C}, \quad (4)$$

$$PD^3 = 8629\ldots \text{m Torr.cm}^3 @ T = 800^{\circ}\text{C}. \quad (5)$$

Equations (2) to (5) are relevant to the deposition conditions tested in our study and are used as the framework for analysis of morphology development during LSMO deposition on Si. Phase evolution is also simultaneously examined in order to define the complete process space for PLD of LSMO directly on Si.

IV. RESULTS AND DISCUSSIONS

A. Obtaining dense LSMO films on Si

1. Morphology evolution

Obtaining high-T_c LSMO films with dense morphology is the first step towards realization of top-down device structures on the Si platform. However, the morphology needs to be carefully engineered since these are lattice-mismatched systems. In this work, morphology evolution with respect to the PD^3 law was evaluated at temperatures ranging from 670 °C to 800 °C. Table I lists key process sets in the high temperature regime along with their calculated PD^3 product values and deviation from their corresponding theoretical constants given by Eqs. (4) and (5). These process sets correspond to deposition conditions for the highest T_c LSMO films obtained on Si, and are representative of the morphology and phase evolution trends also observed at lower deposition temperatures in this study.

We start with process set I at 750 °C, where the PD^3 product is almost equal to its corresponding law constant, with a deviation of only +6%. As per morphology predictions outlined in Sec. III, this is expected to give us dense films with bimodal grain size distribution.[34] Surface SEM micrograph of this film is shown in Figure 1. While the film morphology is dense as expected, grain sizes are seen to vary between ~20 nm to 60 nm. XRD signature of this film in Figure 2 is seen to match XRD pattern of target $La_{0.7}Sr_{0.3}MnO_3$ with rhombohedral perovskite structure, thereby attesting its phase purity and polycrystallinity. Figure 3 captures key information derived from magnetization measurements. Figure 3(a) demonstrates the difference in slope during ferromagnetic to paramagnetic state transition for all samples while Figure 3(b) plots the inverse susceptibility rise at T_c, with the lowest and highest T_c transitions demonstrated within the figure. Table I lists extracted T_c values from magnetometry measurements for all the key process sets. T_c of sample I was found to be 344 K. While this is higher than reported LSMO film T_c values in literature, it is still lower than the expected bulk T_c of 360 K. Reduction in film T_c is possible due to multiple factors such as in-built

Reuse of AIP Publishing content is subject to the terms at: https://publishing.aip.org/authors/rights-and-permissions. Download to IP: 130.102.82.169 On: Tue, 04 Oct 2016 05:47:48

TABLE I. Key PLD process sets, including comparison with PD^3 law constants and characterized data. Values in bold refer to key parameter changes done in each set.

Film/process set	ED [J. cm^{-2}]	SS [cm^2]	RR [Hz]	P [mTorr]	D [cm]	T [°C]	Cooling rate [°C min^{-1}]	PD^3 product [mTorr cm^3]	Deviation from PD^3 constant	Crystal structure[a]	T_c [K]
I	2	0.06	8	135	4.5	750	Natural	12301.88	+6%	R	344
II	2	0.06	8	135	4.5	**800**	Natural	12301.88	+43%	R	350
III	2	0.06	8	**0.11**	4.5	800	Natural	9.1125	−100%	O	348
IV	2	0.06	8	135	4.5	750	**5**	12301.88	+6%	R	349
V	2	0.06	8	135	4.5	800	**5**	12301.88	+43%	R	349
VI	2	0.06	8	0.11	4.5	800	**5**	9.1125	−100%	T	261[b]
VII	2	0.06	8	**275**	4.5	800	5	25059.38	+135%	R	348
VIII	2	**0.02**	10	300	4.5	800	5	27337.50	+217%	R	335
IX	2	0.02	10	300	**5.1**	800	5	39795.30	+361%	R	355

[a]As matched with ICDD XRD database. R stands for rhombohedral, O stands for orthorhombic, and T stands for tetragonal.
[b]The observed transition is tentatively labeled as T_c.

strain, oxygen vacancies, off-stoichiometry, and compositional non-uniformity across the sample.[20,30,39] Since XRD signature indicates the film to be polycrystalline, strain in the film due to texture or epitaxy is ruled out in case of sample I. Additionally, the deposition pressure used in set I is within range of literature reported values that give well-oxygenated films.[38] Of all the probable causes, we estimate compositional non-uniformities across the sample to be most dominant. It is known that substrate temperature T is an important process parameter for preserving the stoichiometry of multi-component oxides with varying elemental vapour pressures since it determines the heat loss of a condensate through the substrate.[40] The lower this temperature, higher is the cooling rate of a fresh condensate on the substrate. The mean ad-atom mobility thereby reduces, leaving only a few ad atoms energetic enough to reach growing crystallites. Temperature of the as-deposited condensate rises when the next pulse of species arrives and unbound atoms (if any) of the more volatile elements in the condensate can re-evaporate, leading to preferential enrichment of the remaining elements. This effect would be more pronounced for systems with high degree of lattice mismatch and high barrier for nucleation, as is the case for LSMO deposition on Si. These conditions can lead to off-stoichiometry and compositional non-uniformities in the subsequent film. With a view to minimize this effect, substrate temperature T in the next process set was increased to 800 °C, while maintaining the rest of the deposition conditions constant. As expected, T_c value of sample II increased to 350 K (Figure 3(b)) while preserving polycrystallinity and phase match with target in its XRD signature (Figure 2). We

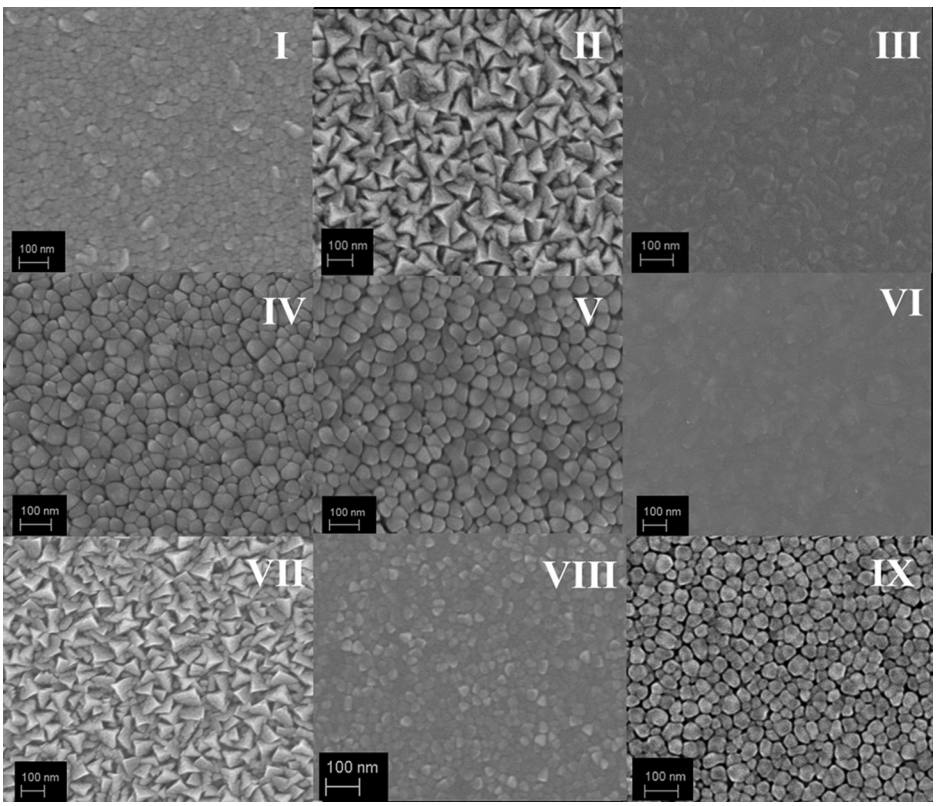

FIG. 1. Surface scanning electron micrographs of films deposited under all the key process sets listed in Table I.

Reuse of AIP Publishing content is subject to the terms at: https://publishing.aip.org/authors/rights-and-permissions. Download to IP: 130.102.82.169 On: Tue, 04 Oct 2016 05:47:48

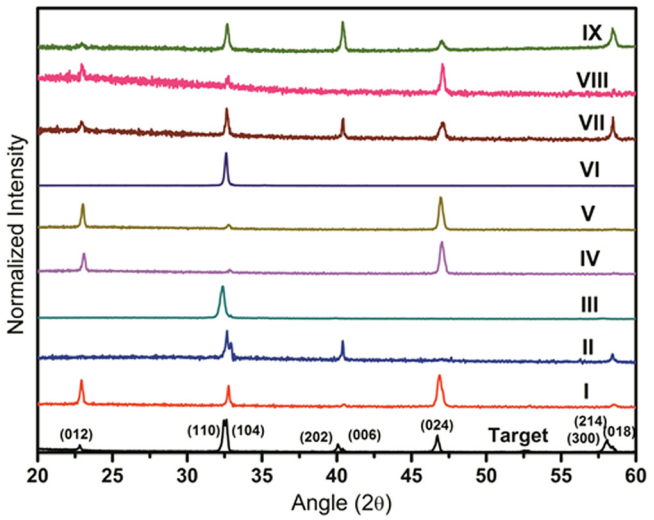

FIG. 2. Normalized XRD data of all the key process set films in comparison with LSMO target XRD signature.

propose that under the given ablation conditions, a high T minimizes loss of stoichiometry and aids crystallite formation of LSMO on Si. Therefore, tuning T for phase quality is equally important while establishing morphology control using PD^3 conditions.

While an increase in T led to improvement in T_c value of sample II, it also changed the surface morphology of the film in comparison to sample I. With an increase in T, the applicable PD^3 law constant for sample II dropped in value—as a result, its PD^3 product deviated from its law constant by +43%. As per morphology predictions quoted in Sec. II, a columnar morphology is expected to emerge due to low ad atom energy on the substrate. Instead, we obtained a mesh of interspersed flaky grains with a wide grain size distribution and rough surface—shown in Figure 1. We refer to this as "transition morphology"—with neither dense grain packing nor columnar grains. Similarly, to check the effect of low PD^3 product value, sample III was deposited at near vacuum conditions while maintaining rest of the conditions as sample II. In this case, PD^3 product deviated from its corresponding law constant value by −100%. Figure 1 demonstrates sample III to possess very dense morphology, indicative of a layer-by-layer 2D growth mode.[36] This "ultra-dense morphology" is in line with predictions outlined in the theoretical section. XRD signature of this film consists of a single peak (Figure 2) that best matches (020) plane of the orthorhombic $La_{0.875}Sr_{0.125}MnO_3$ system—indicative of a highly textured growth.[41] This is expected to lower the film T_c value considerably due to strain in the textured film. However, T_c of this film was found to be as high as 348 K (Figure 3(b)). Unexpected morphology of sample II and unexpected phase signature of sample III point towards an important factor to be considered during PLD of LSMO on Si—formation of metastable microstructures.

One of the unique features of PLD technique is seen when working at a high degree of supersaturation. Unlike other growth processes working at high degrees of supersaturation (such liquid phase epitaxy, where nucleation occurs from supersaturated solid solutions), growth rate under these

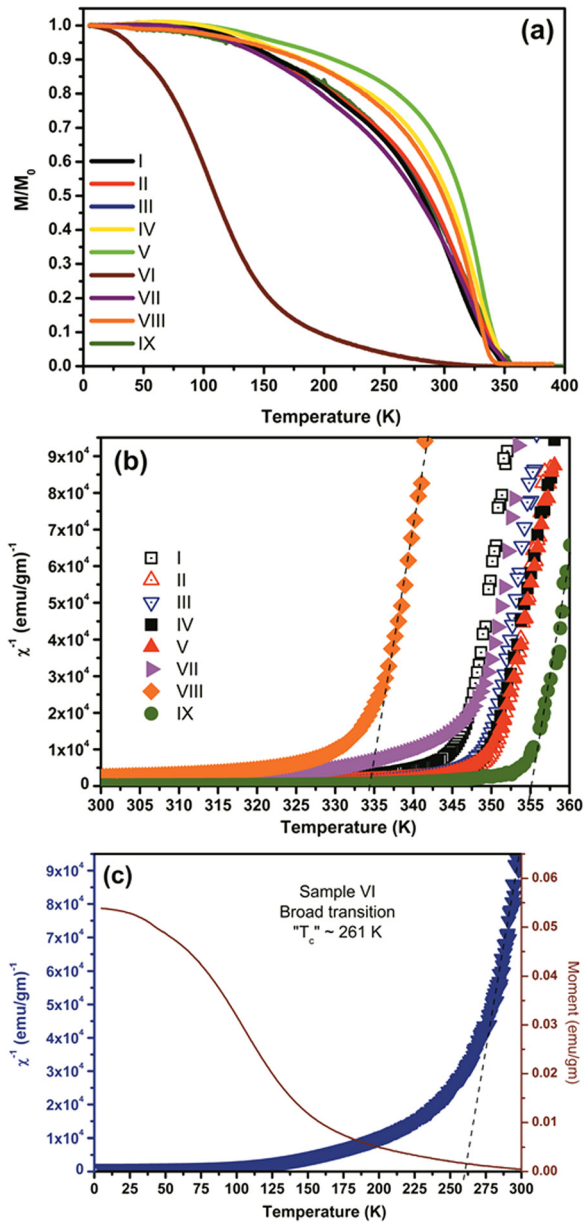

FIG. 3. (a) Normalized magnetization data (M/M_0) from field cooled (at H = 50 Oe) measurements, where M = moment measured at a given temperature, M_0 = moment measured at 5 K. Among all the samples, slow-cooled sample V demonstrates the sharpest transition from its PM to FM state. (b) Determination of Curie temperature by extrapolating the linear section to $\chi^{-1} = 0$ as per the Curie-Weiss law. The dashed lines are shown as an example. (c) As-measured magnetization data of sample VI is plotted (right Y-axis) along with calculated χ^{-1} (left Y-axis) to demonstrate its unusually broad transition over a wide temperature range.

conditions does not drop during PLD. As a result, at high deposition rates and supersaturation conditions, formation of metastable microstructures or phases is highly likely during PLD.[36] As per Greene's theory on growth dynamics for a given film-substrate system, the degree of supersaturation is increased by increasing the pressure of incoming vapour flux on the substrate during deposition.[40] In PLD, for widely differing PD^3 conditions, this criterion can be achieved at high ED and large SS. Reported PLD conditions for LSMO in literature indicate ED to range from 0.35 to 3 J cm^{-2}, with SS ranging from 0.01 to 0.1 cm^2.[42–44] In this light, deposition

Reuse of AIP Publishing content is subject to the terms at: https://publishing.aip.org/authors/rights-and-permissions. Download to IP: 130.102.82.169 On: Tue, 04 Oct 2016 05:47:48

conditions for our samples I to III suggest that at *ED* of 2 J cm^{-2}, *SS* value of 0.06 cm^2 may be high enough to result in a high degree of supersaturation and possibly lead to formation of metastable phases in the film (Table I). Additionally, these metastable microstructures are likely to be frozen if the substrate temperature post-deposition drops suddenly—as is the case for samples I to III, which are naturally quenched post deposition. Hence, although dense grain packing is easily achieved, it is imperative to ensure that films deposited under high supersaturation conditions are phase-stable and repeatable. For the same, samples IV to VI were deposited under identical conditions as I to III, respectively, followed by controlled cooling at the rate of 5 °C min^{-1} post deposition (Table I). Characterization results of these samples are given in Sec. IV A 2.

2. Phase stability check

Among the naturally cooled samples described in Sec. IV A 1, III represented the best process set for a uniformly dense morphology film along with high T_c. Sample VI was obtained under the same process conditions followed by controlled cooling (Table I). Figure 1 shows that it possesses an ultra-dense morphology similar to that of film III. However, it exhibited a drastic drop in T_c value with a very broad magnetic transition spanning 100 K to 300 K, as shown in Figures 3(a) and 3(c). Additionally, the film's XRD signature now best matched with the tetragonal, double-layer perovskite structure of $La_{1.2}Sr_{1.8}Mn_2O_{6.97}$ system.[45] These results indicate that LSMO deposition on Si under high supersaturation and near vacuum conditions leads to the formation of a metastable film. Similar ultra-dense films with impure or unstable phase were obtained at other PD^3 product values lower than the law constant value by a margin greater than −50%. Hence, although these films possess the best morphology for top down device fabrication, their poor phase quality renders them unusable for applications.

Phase-pure, dense films suitable for device applications were obtained only when working close to the PD^3 law conditions—as demonstrated by samples IV and V. These samples were deposited under identical process conditions as sets II and III, respectively, followed by controlled cooling in each case. Surface SEM micrographs of samples IV and V (Figure 1) indicate the film morphologies to have evolved to a dense packing of grains with negligible inter-granular separation on controlled cooling. Stabilization of phase is seen through their T_c values—both having settled at 349 K (Figure 3(b)), while a sharper transition from their paramagnetic to ferromagnetic state also indicates improved domain size uniformity through slow cooling (Figure 3(a)). Their XRD patterns point towards emergence of texture with a preferential orientation along {012} planes (Figure 2). Similar morphology and phase signatures were seen for all PD^3 conditions that lie within |50%| variation from the derived law constant value. All the samples were repeated to re-confirm their measured properties. These results indicate that at a given substrate-target distance *D*, tuning the oxygen ambient pressure *P* to ensure optimal arrival energy of the incoming flux species is critical towards obtaining stable, phase pure films with dense grain packing. These films are best suited for top down device fabrication, satisfying both the critical requirements for all device applications—desired physical properties and assured repeatability.

In order to confirm these properties in the sub-100 nm regime, thin films with average thickness of 50 nm each were deposited using process sets IV and V and characterized thereafter. Surface SEM micrographs of these films revealed them to have identical dense morphologies with tight grain packing as expected. Room temperature XPS measurements on their as-deposited film surfaces were conducted to probe the presence of chemical inhomogeneity. Typical La3d, Sr3d, Mn2p, and O1s core level XPS spectra of the two samples were analyzed and found to be in line with literature reports.[19,46] O1s spectrum was analysed prior to those of the heavier elements since the intrinsic line width of an Mn2p peak is estimated to be higher than that of a O^{2-} peak in the O1s spectrum of manganites.[47] The Mn2p spectrum was seen to consist of two broad peaks—one each at ~642 eV and 653 eV, corresponding to Mn2p3/2 and Mn2p1/2 core levels, respectively. Each of these peaks can be decomposed into contributions from Mn^{2+}, Mn^{3+}, and Mn^{4+} states, especially due to Sr-doping and oxygen content variation in this compound. In line with studies on Mn2p3/2 peak resolution, Mn^{2+}, Mn^{3+}, and Mn^{4+} multiplets were incorporated during curve fit, with a first estimate of their relative intensities and energy splitting as given in literature.[47] The FWHM of all multiplet peaks were maintained at 1.6 eV, while the peak shape was restricted to be 50% Gaussian−50% Lorentzian. Binding energy and intensity values of overlapping multiplet peaks as well as of the lowest energy peak in each multiplet set was set to be variable during curve fit runs. An estimate of Mn^{2+} content relative to Mn^{3+}, and Mn^{4+} was obtained by considering the area under their individual contribution peaks. Magnetic and electronic phase transitions in LSMO are known to arise from the ability of Mn cation to switch between its multivalent states.[8] While Sr-doping leads to fluidity between Mn^{3+} and Mn^{4+} states in the Mn-O-Mn matrix, oxygen vacancies in the film also lead to active Mn^{2+} sites to maintain charge balance. Hence, a higher Mn^{2+} content is indicative of greater concentration of oxygen vacancies and chemical inhomogeneity in the sample. As seen in Figure 4, each Mn2p3/2 peak can be said to consist of two sets of multiplets—ones that arise from simultaneous contribution from multiple Mn valence states, and others that arise individually from specific Mn valence states. From the second set of multiplets, relative Mn^{2+} content is estimated to be higher in set IV, indicating higher deficiency in this sample.

Similar to Mn2p, La3d, and Sr3d core levels also exhibit splitting. Curve fitting was done for La3d5/2 and Sr3d5/2 peaks, maintaining a predominantly Gaussian shape for their primary multiplets. Surface concentrations of individual elements in each sample were calculated by considering area under La3d5/2, Sr3d5/2, and Mn2p3/2 peaks, along with their specific sensitivity factors. As listed in Table II, the surface ratio of La:Mn in set IV is seen to be much higher than the expected bulk value of 0.7. This indicates high La visibility at the surface, possible due to greater degree of oxygen

Reuse of AIP Publishing content is subject to the terms at: https://publishing.aip.org/authors/rights-and-permissions. Download to IP: 130.102.82.169 On: Tue, 04 Oct 2016 05:47:48

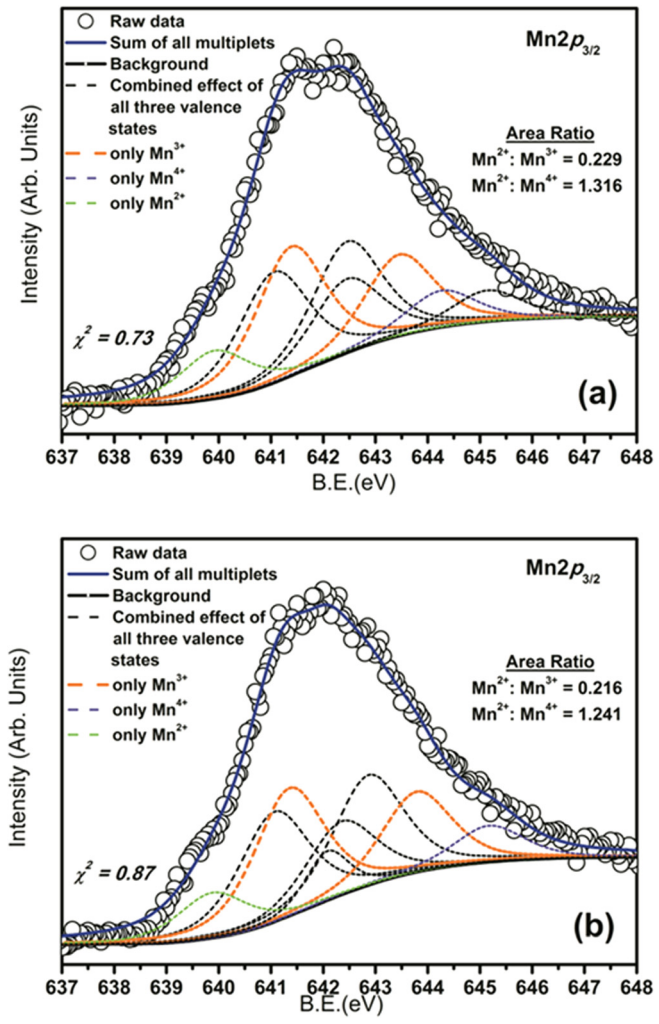

FIG. 4. XPS analysis of Mn2$p_{3/2}$ peak of thin films of process sets (a) IV (b) V. Some multiplet peaks arise due to contribution from all three Mn valence states (Mn^{2+}, Mn^{3+}, and Mn^{4+}), while others correspond to specific valence states. Mn^{2+} content relative to Mn^{3+} and Mn^{4+} is estimated—higher Mn^{2+} content in sample IV is indicative of greater oxygen vacancies in the sample. The chi-square goodness of fit value for both the datasets is also included.

vacancies. For set V, the La:Mn ratio is slightly lower than expected bulk value of 0.7, while the Sr:Mn ratio is higher than the expected bulk value of 0.3. This is in line with literature reports, where Sr segregation at the LSMO surface is often observed.[19] In summary, although both sets IV and V provide identical bulk films morphologically and phase-wise, set V is seen to offer greater chemical homogeneity in the thin film regime owing to its higher deposition temperature T. Therefore, for obtaining device quality dense films at $ED \sim 2\,\mathrm{J\,cm^{-2}}$ and $SS \sim 0.06\,\mathrm{cm^2}$, it is recommended that PLD be performed at highest possible substrate T in tandem with the PD^3 product maintained within |50%| variation from its corresponding law constant. Additionally, a controlled ramp down rate post deposition is recommended for morphology and phase stabilization of LSMO films deposited on Si.

TABLE II. Surface composition (at. %) and cationic ratio of elements in 50 nm LSMO films with dense morphology, calculated from XPS spectra of La3$d_{5/2}$, Sr3$d_{5/2}$, and Mn2$p_{3/2}$.

Film	La	Sr	Mn	La/Mn	Sr/Mn
IV	43.41	17.74	38.86	1.117	0.457
V	29.41	23.56	47.03	0.625	0.501

B. Obtaining columnar LSMO films on Si

1. Tuning the degree of supersaturation

Columnar LSMO films on Si with measurable intergranular separation and high T_c are highly desired for bottom up device applications using this material. In this regard, empirical predictions from previous work based on the PD^3 law suggest depositions at a PD^3 product value that is much greater than the law constant value at a given substrate temperature (see Sec. II). Through our work on dense morphology development, we have seen that depositions at PD^3 product values within |50%| variation from their corresponding law constant and with controlled cooling post-deposition consistently give dense morphology films. Hence, in order to achieve columnar morphology films, we performed depositions at various PD^3 conditions where the product deviation from its law constant was greater than +50%, while also maintaining controlling cooling rate to stabilize the film in phase and morphology.

Process set sample VII was deposited under identical conditions as sample VI, except for the large increase in the oxygen partial pressure P, thereby raising its PD^3 product value upto +135% higher than its corresponding law constant. XRD of this sample was seen to match the polycrystalline rhombohedral structural signature of the target (Figure 2) while its T_c was found to be 348 K (Figure 3(a)). However, surface SEM of this sample revealed a "transition morphology" consisting of a mesh of interspersed flaky grains (Figure 1). This morphology persisted for all depositions attempted with PD^3 product deviation ranging between +50% to +200%, wherein some films also exhibited impurity peaks in XRD. This indicates that mere modification of PD^3 values might not result in a smooth transition between dense and columnar films on Si. Modification of other PLD parameters is necessary to achieve this goal. In order to identify the other key process parameters for this goal, we revisit Greene's theory describing principal conditions that affect growth dynamics for a given film-substrate system.[36] It is well understood that for achieving a columnar morphology, the Volmer-Weber growth mode is preferred—generally manifested in systems with a high degree of lattice mismatch.[23] However, the prime factor that determines a growth mode and consequential morphology evolution is the free energy barrier for nucleation of a film—a higher free energy barrier translates into a lower nucleation density; thereby increasing the probability of obtaining a porous, columnar film. The net free energy barrier for nucleation for a given film-substrate system is directly proportional to interfacial energies (as dominated by the lattice mismatch), while being inversely proportional to supersaturation conditions.[36] Due to widely differing physical properties, mismatch in LSMO-Si system is naturally high and is therefore predisposed to have a high free energy barrier for nucleation. Yet, it is only by tuning the supersaturation conditions that one can

Reuse of AIP Publishing content is subject to the terms at: https://publishing.aip.org/authors/rights-and-permissions. Download to IP: 130.102.82.169 On: Tue, 04 Oct 2016 05:47:48

obtain transition between dense and columnar morphologies of the deposited films.

Across differing PD^3 conditions, the degree of supersaturation can be maintained to be low or high as desired by modulating *ED* and *SS* values. Section IV A 1 postulates how an *SS* of 0.06 cm^2 at a fixed *ED* of 2 J cm^{-2} is proposed to provide a high degree of supersaturation, thereby giving dense morphology LSMO films on a lattice mismatched Si substrate. Therefore, we now reduce the *SS* value in tandem with a high PD^3 product value in order to achieve phase pure, columnar films. Maintaining the same *ED* values, a decrease in *SS* can provide a monotonic drop in plume flux density and velocity, thereby reducing the degree of supersaturation.[36] Additionally, in order to reduce the relaxation time vs. species arrival rate at the substrate, the laser pulse *RR* was increased to 10 Hz. This is expected to aid in the nucleation of separated 3D islands, thereby leading to a preferential Volmer-weber growth mode. Process set sample VIII was deposited under these modified supersaturation conditions, with the primary change being the drop in SS (Table I). Surface SEM inspection of this sample revealed columnar grains (average size ~18 nm) with low inter-granular separation (see Figure 1). XRD and magnetometry measurements confirmed the film to be polycrystalline rhombohedral LSMO with T_c of 335 K (Figures 2 and 3(b)). Although lack of distinct inter-granular separation makes this sample unsuitable for bottom up device applications, it proves the necessity for modification of degree of supersaturation along with PD^3 conditions for emergence of a columnar morphology.

2. Tuning the substrate-target distance

Although sample VIII marked the emergence of columnar morphology, it exhibited very low inter-granular separation (<5 nm). For bottom-up device applications, a porous film with well-separated columnar grains is desired. Hence, in order to achieve greater inter-granular separation, the PD^3 product deviation was increased further for the next deposition while maintaining a low *SS*. However, this time, a higher PD^3 product value was achieved by varying *D* instead of *P*.

Third order dependence of parameter *D* in the PD^3 law suggests that morphology of a deposited film is likely to be more sensitive to changes in *D* than changes in *P*. In a detailed study by Strikovski *et al.*, a characteristic distance called the "plume range" L_0 was defined to be the distance over which all the species in the plume get thermalized.[48] L_0 is dependent on the ambient pressure *P*, and is argued to be the distance at which the species arrival velocity is adequate for surface activation. It has been shown in the same study that to maintain constant arrival velocity of species, a change in pressure by a factor of 2 would require changing the distance upto 2 cm. In this light, we increased the PD^3 deviation upto +361% for sample IX by increasing the *D* value by only 0.6 cm (Table I). The resultant film was found to exhibit the desired columnar morphology, with a distinct inter-granular separation around 10 nm (Figure 1). XRD micrograph of this polycrystalline sample matched the LSMO target rhombohedral structure (Figure 2). Of all the deposited films, sample IX exhibited the highest T_c of 355 K on Si (Figure 3(b)). Both XRD and magnetometry results indicate a phase pure film with only 1.4% reduction in T_c value from the bulk value of 360 K, possible due to residual strain in the film. While strain due to lattice mismatch is minimized in case of relaxed, polycrystalline columnar films; strain due to difference in thermal expansion between Si and LSMO is incorporated in the film when it is cooled down to room temperature post deposition. Consequently, for all high temperature depositions on Si, we expect non-zero residual strain to be present in LSMO films, irrespective of other process conditions.

Data presented above suggests that in order to transition from a dense to columnar morphology[49] for device fabrication, two key conditions need to be satisfied—PD^3 product to be higher than the law constant, and low degree of supersaturation (achieved at low *SS*). Additionally, it reveals that tuning *D* (instead of only *P*) to achieve the requisite large PD^3 product value serves to more effective in achieving device quality, columnar films. High T_c is also achieved under these conditions.

C. Engineered PLD process space

1. Morphology zones in accordance with the PD^3 law

Process sets described in Table I and their characterization results have been used to illustrate the evolution of morphology and phase stability seen through our experiments at 800 °C. Additional process sets were also executed at differing PD^3 conditions and temperatures, and characterized thereafter. On data collation, we find that morphology "zones" can be defined in accordance with the PD^3 law constant. These zones provide a map to estimate resultant morphology and phase of films deposited at various *P* and *D* values.

Figure 5(a) illustrates the morphology zones defined through our experimental results at 800 °C—for ultra-dense, dense, transition, and columnar morphology LSMO films on Si. These zones were essentially defined through a PD^3 contour plot and zone boundaries were specified in accordance with the PD^3 law constant at 800 °C, i.e., 8629 mTorr cm^3 (derived in Sec. II). Zone "D," defined within |0.5| times the law constant value, gives phase-pure films with dense grain packing suitable for top-down device fabrication. A high *SS* ($\geq$0.06 cm^2) is essential for this region and across its boundaries. Above and below this region lie zones "Tr" and "Ultra-D," respectively—both of which often result in films with phase impurities or instability, and therefore unsuitable for device applications. Beyond the transition zone lies zone "C" where phase-pure, columnar films can be obtained only with low *SS* ($\leq$0.02 cm^2). Inter-granular separation between the columns can be improved operating at higher *D* values, thereby making the films more suitable for bottom-up device applications. Boundary position between zones "Tr" and "C" is dependent on values of *SS* and *D*. As *SS* is reduced, this boundary is expected to shift to the left while a reduction in *D* is expected to shift the boundary to the right. At *SS* of 0.02 cm^2 and *D* of 5.1 cm, columnar morphology films are seen to

Reuse of AIP Publishing content is subject to the terms at: https://publishing.aip.org/authors/rights-and-permissions. Download to IP: 130.102.82.169 On: Tue, 04 Oct 2016 05:47:48

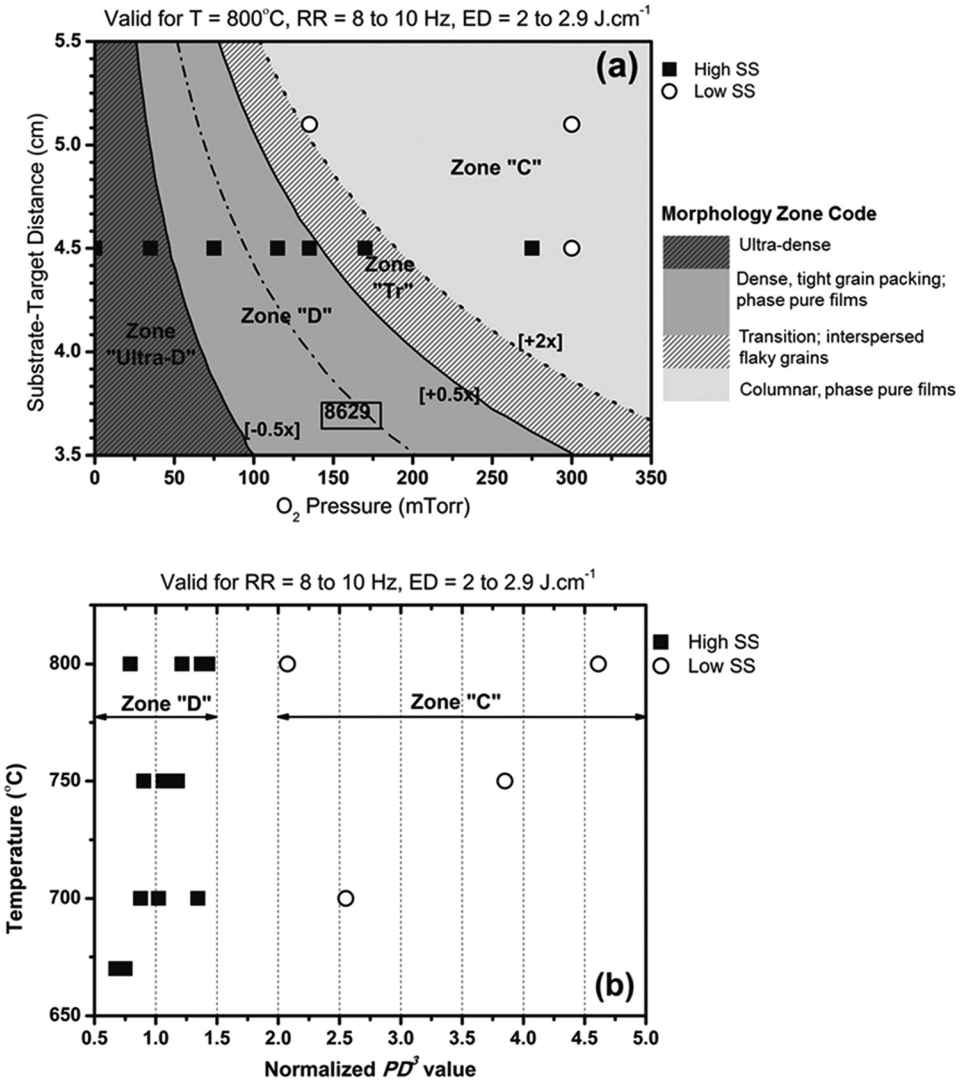

FIG. 5. (a) Morphology zones for LSMO films deposited directly on Si at 800 °C, in accordance with the PD^3 law constant at 800 °C, i.e., 8629 mTorr cm^3. The hashed zones denote high probability for phase instability/impurity. Dense packing of grains and phase purity is seen for PD^3 conditions within 50% variation from the law constant. Above 50%, the morphology slowly transitions into distinct columnar grains—range of this transition zone is strongly dependent on SS and D. In this diagram, zone "Tr" boundary has been placed at 200%, based on columnar films obtained for low SS and D = 5.1 cm. (b) Validation of the PD^3 morphology zones at various temperatures for dense and columnar device films.

emerge when PD^3 conditions are greater than twice the law constant—this is illustrated as the dashed line boundary between zones "Tr" and "C" in Figure 5. Validity of all zones defined in this figure has been ascertained across *ED* variation from 2 to 2.9 J cm^{-2}. This indicates SS to be a more effective PLD parameter than *ED* for tuning the degree of supersaturation and therefore the resultant morphology of deposited films.

Through our experiments at 670 °C, 700 °C, and 750 °C, identical morphology evolution trends have been observed in accordance with their corresponding PD^3 law constants. Validation of our defined boundaries for zone "D" and zone "C" is demonstrated in Figure 5(b). This suggests that individual morphology zone diagrams can be constructed for other deposition temperatures as well to predict film morphology at various *P* and *D* conditions.

2. Phase evolution with energy density and temperature

As demonstrated through Figure 5, morphology within every zone is insensitive to *ED* variation from 2 to 2.9 J cm^{-2}. However, the effect of *ED* variation on the phase of the deposited films needs to be closely examined. With this goal, zone "D" morphology films of various temperatures and deposited at various *ED* values were examined for phase quality through their XRD and magnetometry measurements. As labeled in Figure 6(a), all samples exhibited high T_c values, i.e., $T_c \geq 340$ K. However, an interesting trend was observed in their XRD results—as the deposition temperature increased from 670 °C to 800 °C, films deposited at lower *ED* values exhibited preferential orientation along {012} planes. This is demonstrated in Figure 6(b) through XRD results of zone "D" films deposited at 800 °C. At *ED* of 2.9 J cm^{-2}, the deposited film exhibits clear signs of polycrystallinity with multiple peaks observed in its XRD result. However, as one proceeds to 2 J cm^{-2}, only 3 peaks corresponding to planes (012), (110), and (024) are observed in the deposited film, with maximum intensity seen for (012) and (024) signatures. This result indicates an emergence of texture along {012} family of planes, reported for the first time for LSMO films deposited directly on Si. Through texture observation in XRD data at all temperatures,[49] an inverse relationship between *ED* and *T* is suggested—as obtained via a second order polynomial fit in Figure 6(a). A possible cause underlying this inverse relationship is suggested below.

Independent studies have proposed plume flux to be a two-component system, containing a broad thermal component with cos θ dependence, along with a second component

Reuse of AIP Publishing content is subject to the terms at: https://publishing.aip.org/authors/rights-and-permissions. Download to IP: 130.102.82.169 On: Tue, 04 Oct 2016 05:47:48

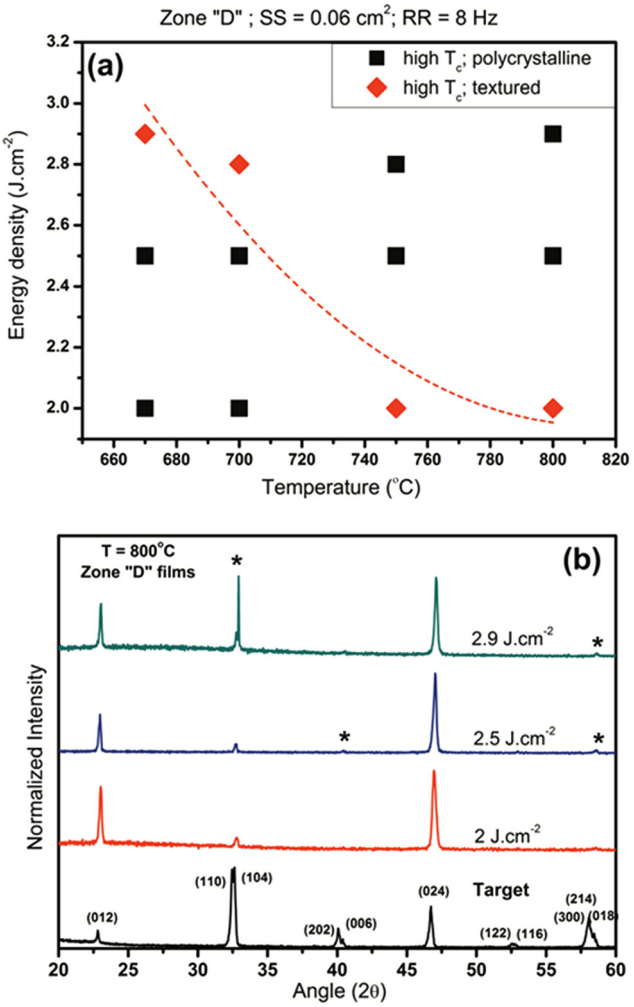

FIG. 6. (a) Map of high T_c (i.e., $T_c > 340$ K) dense morphology LSMO films obtained on Si at various energy density and temperature conditions. An additional advantage of texture formation is seen to emerge—the dashed line is a 2nd order polynomial fit highlighting the inverse relationship between energy density and temperature for textured films. (b) An example of emergence of texture as seen through XRD results of zone "D" films at 800 °C. At 2 J cm^{-2}, preferred orientation along {012} planes is seen to have developed. The starred peaks highlight other planes whose signature has either diminished or vanished at 2 J cm^{-2}.

with higher forward peaking and *ED*-dependent intensity.[50] A process in zone "D" operates close to the plume range, wherein most of the plume species are thermalized and individual velocities of the plume species would be dependent on their mass. In the model proposed by Saenger[51] and verified experimentally for YBCO by Venkatesan *et al.*,[52] transition from a "weak expansion regime" to a "strong expansion regime" is proposed to take place with increasing *ED*, depending on Mach numbers of the plume species. In the weak expansion regime, i.e., at low *ED*, the higher collision rate of light species imparts them higher flow velocities than their heavier counterparts. Whereas in the strong expansion regime, i.e., at high *ED*, all species will tend to have the same flow velocity and local temperature due to very large number collisions in a highly dense plume. However, the higher mass species can gain higher thermal velocities owing to their mass advantage, leading to their on-axis enrichment.[52] Such chemical inhomogeneity would be aided if substrate *T* is also high, due to high ad-atom mobility and higher growth rate of on-axis non-stoichiometric clusters. Hence, while operating at high *ED*, a low substrate *T* would be preferable to reduce energy of high mass species and nucleation probability for non-stoichiometric clusters. On the other hand, while operating at lower *ED* (i.e., the weak expansion regime), high velocities of the low mass species can be reduced via collisions with ambient gas. Ambient gas collisions are known to be more effective in reducing velocities of the lower mass species in the plume whose masses are comparable with those of O_2 molecules. This is effective when working at sufficient O_2 pressure ambient (i.e., plume range conditions), ensuring comparable local velocities of all incoming elemental species. When coupled with a high substrate *T*, growth of stoichiometric clusters is further aided. These conditions are therefore proposed to assist high degree of chemical and structural homogeneity in the deposited films.

3. Implications for device applications

Put together, Figures 5 and 6 define the complete PLD process space for morphology-controlled, high T_c LSMO films directly on Si. Morphology zones based on *PD*[3] and *SS* conditions have been defined to obtain dense as well as columnar films at any given deposition temperature. Additionally, for dense films, an inverse *ED-T* relationship has also been identified for preferential orientation and texture formation in the deposited films. The laser pulse *RR* is recommended to be maintained within 8–10 Hz as lower repetition rates have been found to give phase impure films. In summary, all PLD process parameters have been unambiguously defined for morphology and phase control along with assured repeatability for LSMO on Si. It is known that device fabrication using these films also requires development of subsequent process modules that are compatible with conventional silicon processing techniques. In this regard, appreciable progress has already been made by various groups in development of processes for LSMO patterning, etching, and metallization.[53–55] With film deposition process control also in place, LSMO-Si device structures for various applications can now be attempted using top-down or bottom-up patterning approaches.

As one proceeds towards device fabrication using LSMO films on Si, a couple of points are to be additionally noted: (i) When working with doped silicon substrates and processes, thermal budgets are often limited. As per applicable constraints, one may need to choose the appropriate *ED-T* process window or work with rapid anneals to obtain the desired film morphology and phase. (ii) If the silicon substrate forms an active part of the device (for example: spin injection applications), detailed investigation into the physical, chemical, and electrical properties of the LSMO-Si interface is required. These interface studies are currently in progress.

V. CONCLUSIONS

We have defined PLD process parameter regimes for direct deposition of LSMO films on Si, with complete

Reuse of AIP Publishing content is subject to the terms at: https://publishing.aip.org/authors/rights-and-permissions. Download to IP: 130.102.82.169 On: Tue, 04 Oct 2016 05:47:48

control over film morphology and phase. PD^3 law constants were derived for our experiments based on earlier reports and thereafter experimentally evaluated for their validity. The laser pulse *SS* was found to play a critical role along with the PD^3 law in establishing morphology control for the lattice mismatched LSMO-Si system. Using PD^3 conditions, morphology zones were defined that can now enable device engineers to choose deposition pressure and distance values at any given substrate temperature for bottom-up and top-down device fabrication. Within each defined zone, film morphology was found to be insensitive to energy density variation. However, an inverse *ED-T* relationship was identified for emergence of texture in dense LSMO films deposited directly on Si. Additionally, all dense and columnar phase-pure LSMO films deposited using these defined conditions were found to exhibit $T_c \geq 340$ K—highest reported for LSMO films on Si so far.

In view of LSMO patterning methods already reported in literature, this work opens up multiple device fabrication possibilities for a wide range of applications. Since reproducibility of these process sets was also confirmed experimentally, statistical studies on performance of devices fabricated using these films can further be designed. It is expected that this work will aid the inclusion of LSMO-based devices in conventional silicon processing, while also providing a framework to design, execute, and evaluate new device concepts using LSMO on the silicon platform.

ACKNOWLEDGMENTS

The authors would like to thank IRCC, IIT-Bombay for providing PPMS VSM and ESCA characterization facilities. This research was performed at Centre of Excellence in Nanoelectronics, IIT-Bombay funded by MCIT, Government of India.

[1]D. M. Brown, M. Ghezzo, and J. M. Pimbley, Proc. IEEE **74**, 1678 (1986).
[2]Y. Taur, IBM J. Res. Dev. **46**, 213 (2002).
[3]P. Avouris, Z. Chen, and V. Perebeinos, Nat. Nanotechnol. **2**, 605 (2007).
[4]A. K. Geim and K. S. Novoselov, Nature Mater. **6**, 183 (2007).
[5]R. Pillarisetty, Nature **479**, 324 (2011).
[6]R. M. Wallace and G. D. Wilk, Crit. Rev. Solid State Mater. Sci. **28**, 231 (2003).
[7]W. Prellier, P. Lecoeur, and B. Mercey, J. Phys. Condens. Matter **13**, R915 (2001).
[8]C. N. R. Rao and A. K. Raychaudhuri, *Colossal Magnetoresistance, Charge Ordering and Related Properties of Manganese Oxides* (World Scientific, Singapore, 1998), Ch. 1.
[9]R. Mahendiran, S. K. Tiwary, A. K. Raychaudhuri, T. V. Ramakrishnan, R. Mahesh, N. Rangavittal, and C. N. R. Rao, Phys. Rev. B. Condens. Matter **53**, 3348 (1996).
[10]C. Mitra, G. Koübernik, K. Doürr, K.-H. Muüller, L. Schultz, P. Raychaudhuri, R. Pinto, and E. Wieser, J. Appl. Phys. **91**, 7715 (2002).
[11]P. K. Siwach, H. K. Singh, and O. N. Srivastava, J. Phys. Condens. Matter **20**, 273201 (2008).
[12]T. Zhao, S. B. Ogale, S. R. Shinde, R. Ramesh, R. Droopad, J. Yu, K. Eisenbeiser, and J. Misewich, Appl. Phys. Lett. **84**, 750 (2004).
[13]P. Han, K. Jin, H. Lu, Q. Zhou, Y. Zhou, and G. Yang, Appl. Phys. Lett. **91**, 182102 (2007).
[14]C. Thiele, K. Dorr, W.-M. Lin, K.-H. Muller, and L. Schultz, Sens. Actuators, A **129**, 180 (2006).
[15]N. A. Morley, H. R. H. Al Qahtani, M. H. Hodges, M. R. J. Gibbs, M. Grell, V. Dediu, and D. J. Morgan, Appl. Surf. Sci. **265**, 570 (2013).
[16]D.-W. Kim, D. H. Kim, T. W. Noh, E. Oh, H. C. Kim, and H.-C. Lee, Solid State Commun. **121**, 631 (2002).
[17]S. Liu, B. Guillet, A. Aryan, C. Adamo, C. Fur, J.-M. Routoure, F. Lemarié, D. G. Schlom, and L. Méchin, Microelectron. Eng. **111**, 101 (2013).
[18]H. R. Shanks, P. D. Maycock, P. H. Sidles, and G. C. Danielson, Phys. Rev. **130**, 1743 (1963).
[19]M. Soltani, M. Chaker, X. X. Jiang, D. Nikanpour, and J. Margot, J. Vac. Sci. Technol. A **24**, 1518 (2006).
[20]D. R. Sahu, D. K. Mishra, J. Huang, and B. K. Roul, Physica B **396**, 75 (2007).
[21]J. Mona, S. N. Kale, R. J. Choudhary, and D. M. Phase, Appl. Phys. Lett. **92**, 142109 (2008).
[22]Si, Int. Cent. Diffr. Data Database, PDF number 00-027-1402.
[23]T.-M. Chang and E. A. Carter, Surf. Sci. **318**, 187 (1994).
[24]$La_{0.7}Sr_{0.3}MnO3$, Int. Cent. Diffr. Data Database, PDF number 01-071-5288.
[25]K. Lord, D. Hunter, T. M. Williams, and A. K. Pradhan, Appl. Phys. Lett. **89**, 052116 (2006).
[26]K. Zhao, K. Jin, H. Lu, Y. Huang, Q. Zhou, M. He, Z. Chen, Y. Zhou, and G. Yang, Appl. Phys. Lett. **88**, 141914 (2006).
[27]J. Qiu, K.-J. Jin, P. Han, H. Lu, C. Hu, B. Wang, and G. Yang, Eur. Phys. Lett. **79**, 57004 (2007).
[28]P. Perna, L. Mechin, M. P. Chauvat, P. Ruterana, C. Simon, and U. S. di Uccio, J. Phys. Condens. Matter **21**, 306005 (2009).
[29]I. Bergenti, V. Dediu, E. Arisi, M. Cavallini, F. Biscarini, C. Taliani, M. de Jong, C. Dennis, J. Gregg, M. Solzi, and M. Natali, J. Magn. Magn. Mater. **312**, 453 (2007).
[30]T. Kanki, H. Tanaka, and T. Kawai, Phys. Rev. B **64**, 224418 (2001).
[31]M. Lippmaa, N. Nakagawa, M. Kawasaki, S. Ohashi, and H. Koinuma, Appl. Phys. Lett. **76**, 2439 (2000).
[32]O. Gautreau, C. Harnagea, F. Normandin, T. Veres, and A. Pignolet, Thin Solid Films **515**, 4580 (2007).
[33]H. S. Kim and H. S. Kwok, Appl. Phys. Lett. **61**, 2234 (1992).
[34]M. Koubaa, A. M. Haghiri-Gosnet, R. Desfeux, P. Lecoeur, W. Prellier, and B. Mercey, J. Appl. Phys. **93**, 5227 (2003).
[35]S. Maity, A. Dhar, S. K. Ray, and D. Bhattacharya, J. Phys. Chem. Solids **72**, 804 (2011).
[36]J. S. Horwitz and J. A. Sprague, *Pulsed Laser Deposition of Thin Films* (John Wiley & Sons, Inc, New York, U.S.A., 1994), Ch. 8.
[37]R. H. Hammond and R. Bormann, Physica C **162–164**, 703 (1989).
[38]M. Koubaa, A. M. Haghiri-Gosnet, P. Lecoeur, W. Prellier, and B. Mercey, Mater. Res. Soc. Symp. Proc. **690**, F9.9.1–F9.9.6 (2001).
[39]J. Dho, N. H. Hur, I. S. Kim, and Y. K. Park, J. Appl. Phys. **94**, 7670 (2003).
[40]S. Metev, *Pulsed Laser Deposition of Thin Films* (John Wiley & Sons, Inc, New York, U.S.A., 1994), Ch. 9.
[41]$La_{0.875}Sr_{0.125}MnO3$, Int. Cent. Diffr. Data Database, PDF number 01–088-0061.
[42]B. Kim, D. Kwon, J. H. Song, Y. Hikita, B. G. Kim, and H. Y. Hwang, Solid State Commun. **150**, 598 (2010).
[43]H. Boschker, M. Mathews, P. Brinks, E. Houwman, A. Vailionis, G. Koster, D. H. A. Blank, and G. Rijnders, J. Magn. Magn. Mater. **323**, 2632 (2011).
[44]L. F. Kourkoutis, J. H. Song, H. Y. Hwang, and D. A. Muller, Proc. Natl. Acad. Sci., U.S.A. **107**, 11682 (2010).
[45]$La_{1.2}Sr_{1.8}Mn_2O6.97$, Int. Cent. Diffr. Data Database, PDF number 00-051-0117.
[46]W. Rao and J. Yu, Adv. Mater. Res. **150–151**, 908 (2010).
[47]H. W. Nesbitt and D. Banerjee, Am. Mineral. **83**, 305 (1998); available at http://www.minsocam.org/msa/ammin/TOC/Articles_Free/1998/Nesbitt_p305-315_98.pdf.
[48]M. Strikovski and J. H. Miller, Appl. Phys. Lett. **73**, 1733 (1998).
[49]See supplementary material at http://dx.doi.org/10.1063/1.4862909 for cross section SEM micrographs and XRD results.
[50]K. L. Saenger, *Pulsed Laser Deposition of Thin Films* (John Wiley & Sons, Inc., New York, U.S.A., 1994), Ch. 7.
[51]K. L. Saenger, J. Appl. Phys. **70**, 5629 (1991).
[52]T. Venkatesan, X. D. Wu, a. Inam, and J. B. Wachtman, Appl. Phys. Lett. **52**, 1193 (1988).
[53]F. Gaucher, A. Pautrat, S. Autier-laurent, C. David, L. E. Calvet, P. Lecoeur, and A.-M. Haghiri-gosnet, Microelectron. Eng. **86**, 820 (2009).
[54]M. Naoe, K. Hamaya, N. Fujiwara, T. Taniyama, Y. Kitamoto, and Y. Yamazaki, J. Magn. Magn. Mater. **235**, 223 (2001).
[55]R. Rajagopal, S. N. Kale, N. A. Raorane, R. Pinto, and V. R. Rao, IEEE Electron Device Lett. **32**, 402 (2011).

Reuse of AIP Publishing content is subject to the terms at: https://publishing.aip.org/authors/rights-and-permissions. Download to IP: 130.102.82.169 On: Tue, 04 Oct 2016 05:47:48